**Structural Engineering and Mechanics**, *Vol. 67, No. 3 (2018) 301-310*
DOI: https://doi.org/10.12989/sem.2018.67.3.301


# Metamodel based multi-objective design optimization of laminated composite plates

Kanak Kalita*[1], Pratik Nasre[1], Partha Dey[2] and Salil Haldar[1]

[1]*Department of Aerospace Engineering and Applied Mechanics, Indian Institute of Engineering Science and Technology, Shibpur, Howrah 711 103, India*
[2]*Department of Mechanical Engineering, Academy of Technology, Adisaptagram, Hooghly 712 121, India*

*(Received March 6, 2018, Revised May 8, 2018, Accepted May 25, 2018)*

**Abstract.** In this paper, a multi-objective multiparameter optimization procedure is developed by combining rigorously developed metamodels with an evolutionary search algorithm—Genetic Algorithm (GA). Response surface methodology (RSM) is used for developing the metamodels to replace the tedious finite element analyses. A nine-node isoparametric plate bending element is used for conducting the finite element simulations. Highly accurate numerical data from an author compiled FORTRAN finite element program is first used by the RSM to develop second-order mathematical relations. Four material parameters- $\frac{E_1}{E_2}$, $\frac{G_{12}}{E_2}$, $\frac{G_{23}}{E_2}$ and $\upsilon_{12}$ are considered as the independent variables while simultaneously maximizing fundamental frequency, $\lambda_1$ and frequency separation between the 1st two natural modes, $\lambda_{21}$. The optimal material combination for maximizing $\lambda_1$ and $\lambda_{21}$ is predicted by using a multi-objective GA. A general sensitivity analysis is conducted to understand the effect of each parameter on the desired response parameters.

**Keywords:** FE-surrogate; finite element; multi-objective; optimization; robust model

## 1. Introduction

Favorable qualities like high strength-weight and high stiffness-weight ratios combined with low operational cost have led to increased use of composites in the structural engineering field. Often, these composite structures act as the load carrying members and thus are subjected to various static and dynamic loads (Kalita and Haldar 2017). Therefore it is desirable that any machinery installed on these structures are not in resonance with it. An easy way to ensure this is by allowing the machinery to operate well outside the range of the inherent frequency of the structure. As such the ability to fine tune structures so as to maximize or minimize its natural frequencies would be a handy option for design engineers (Kalita *et al*. 2018).

With rapid advancement in computing power, there has been a competitive development of numerical tools and theories in structural optimization field. A plethora of nature-inspired optimization techniques have been developed in the last three decades to solve multimodal and computationally intensive optimization problems using heuristic approaches. While well-tuned metaheuristics are known to escape the pit of local optima—a serious drawback of classical optimization techniques, many of these metaheuristics (Boussaid *et al*. 2013) are known to depend on several parameters to be set by the user *a priori*, the choice of which considerably influences the success of the approach. For example, in case of Genetic Algorithm, a nature-inspired technique that has been around for almost four decades now, there is still considerable disagreement (Mills *et al*. 2015) amongst researchers regarding the various tuning parameter settings. In fact, De Jong (2007) suggested that any numerical experimentation based on evolutionary algorithms should first conduct a few preliminary experiments to determine the optimal parameter setting. Additionally, to gain sufficient confidence in the predicted output, often an optimization problem needs to be solved multiple times using several combinations of the tuning parameters involved in the particular metaheuristics. Though this can be easily done for problems involving a small number of parameters and small search space, in structural optimization problems involving finite element simulations this can be a tedious and time-consuming option. Finite element approaches are known to be accurate but are computationally intensive.

A remarkable reduction in the total computational effort can be obtained by reducing the number of structural analyses. This can be done by developing globally robust approximation routines. Such an approximation routine or metamodel eliminates the linkage of finite element and optimization algorithm codes (Abu-Odeh and Jones 1998), thereby eliminating the need to run the computationally intensive FE models iteratively. By replacing the original FE model with a metamodel, the objective function can be evaluated at a fraction of the original cost (Pajunen and Heinonen 2014). Response surface methodology (RSM) (Box and Wilson 1992), artificial neural network (ANN) (Haykin 2001) and radial basis functions (RBF) (Hardy 1971) are some of the most popular and widely studied metamodeling techniques. In RSM, the basic functions for

*Corresponding author
E-mail: kanakkalita02@gmail.com



ISSN: 1225-4568 (Print), 1598-6217 (Online)

approximation are chosen *a priori*. RSMs use polynomial basis functions and have been widely used in structural optimization problems like helicopter rotor (Ganguli 2002), truss (Ju *et al*. 2013) (Fang and Tee 2017), stiffened plates (Heinonen and Pajunen 2011), marine structures (Pajunen and Heinonen 2014), laminated plates subject to stress and displacement constraints (Abu-Odeh and Jones 1998), lateral stability of arch bridge (Pan *et al*. 2011), FRP composite deck (Kim *et al*. 2009) (Mukhopadhyay *et al*. 2015) (Mukhopadhyay *et al*. 2015) (Dey *et al*. 2015) composite plates (Abu-Odeh and Jones 1998) and shells (Dey *et al*. 2016), etc.

Though the literature search reveals that RSM metamodels are effective in structural engineering, it also initiates the necessity to explore further. One interesting avenue is to test its applicability in a multi-objective optimization scenario. In tune with genetically modified organisms whose genetic material is altered to increase yield or for some other specific purpose, the present research work explores genetically optimized composite laminates, whose material properties have been altered with the help of the in-silico counterpart of genetic engineering, viz. genetic algorithm, to simultaneously maximize the fundamental frequency and frequency separation between first two natural modes. This paper is organized as- section 1 details the necessity and scope of the research. Section 2 presents a brief overview of the overall design and optimization framework. The finite element formulation and response surface model used in the research is discussed in detail to ensure reproducibility. A small discussion regarding genetic algorithms is also included. In section 3, the FE model is validated with published results. The RSM model is discussed and a general sensitivity analysis is also carried out. The RSM-based second order equations built to replace the FE model are then used as objective functions in a multi-objective GA in the final part of section 3. Section 4 lists the key findings and recommendations.

## 2. Design and optimization framework

Traditionally, finite element analysis (FEA) is directly coupled with optimization algorithms to predict the optimal settings. However, due to the time intensive nature of FEA, the optimization scheme may take hours or days (depending on model complexity and dimensionality) to converge to an optimal solution. By replacing the FEA with a metamodel, this can be done in a fraction of the actual computational cost. For example, if an optimization algorithm needs 50,000 iterations to converge to an optimal solution, the function evaluation would need the FEA to run 50,000 times. However, if suppose say the FEA is replaced with a second-order polynomial equation, the 50,000 function evaluations would take very little time. But, it should be noted that to build the metamodel, a training dataset is necessary which in structural engineering is often generated by using FEA. However, the size of training dataset needed in RSM is very small. For example, for a 4-variable design problem, RSM CCD needs only 30 design points. An additional advantage of using an RSM metamodel with optimization algorithms in place of using FEA directly includes ease of conducting sensitivity analysis.

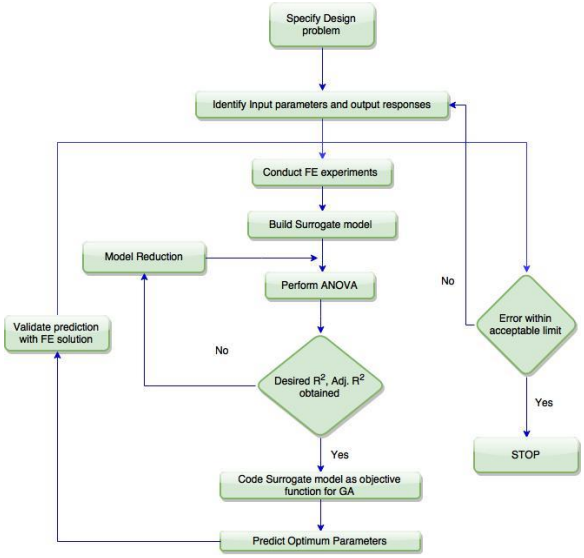


Fig. 1 Design and optimization framework used in the current study

In this article, a multi-objective multiparameter optimization procedure is developed by combining response surface models with an evolutionary search algorithm-GA. The RSM metamodels are developed by using the highly accurate numerical data from an author compiled finite element program. Fig. 1 shows the design and optimization framework for the current problem. Based on the design problem, the input (in this case $\frac{E_1}{E_2}$, $\frac{G_{12}}{E_2}$ , $\frac{G_{23}}{E_2}$ and $\upsilon_{12}$) and output parameters (fundamental frequency, $\lambda_1$ and frequency separation between the 1st two modes, $\lambda_{21}$) are identified. A design of experimentation scheme based on the RSM design (described in section 2.2) is selected and the numerical experiments are conducted using the finite element formulation reported in section 2.1. Metamodels (also called surrogate model) are developed based on these RSM sample points using the FE data. The model is tested for the desired level of accuracy and analysis of variance (ANOVA) test is performed to remove the non-significant terms from the metamodel. The metamodel is then used as the objective function for the multi-objective optimization using a genetic algorithm.

### *2.1 Finite element formulation*

In the current formulation, the finite element method is used for free vibration of the plate. The midplane of the plate of the element is regarded as the reference plane. Since composites are weak in shear, the shear deformation effect is accounted for here. This is done by using the theory of Mindlin plate where it is assumed that the normal to the central plane of the plate before bending remains straight but not necessarily normal to the deformed middle surface after bending (Kalita and Haldar 2017) (Kalita *et al*. 2018) (Kalita *et al*. 2016).

A nine-node isoparametric plate bending element is used in the current finite element formulation. One of the main

Table 1 Design points patterned by CCD

| Trial No. | Coded Inputs | | | | Un-coded Inputs | | | |
|---|---|---|---|---|---|---|---|---|
| | $\frac{E_1}{E_2}$ | $\frac{G_{12}}{E_2}$ | $\frac{G_{23}}{E_2}$ | $\upsilon_{12}$ | $\frac{E_1}{E_2}$ | $\frac{G_{12}}{E_2}$ | $\frac{G_{23}}{E_2}$ | $\upsilon_{12}$ |
| 1 | -1 | -1 | -1 | -1 | 30 | 0.5 | 0.4 | 0.22 |
| 2 | 1 | -1 | -1 | -1 | 50 | 0.5 | 0.4 | 0.22 |
| 3 | -1 | 1 | -1 | -1 | 30 | 0.7 | 0.4 | 0.22 |
| 4 | 1 | 1 | -1 | -1 | 50 | 0.7 | 0.4 | 0.22 |
| 5 | -1 | -1 | 1 | -1 | 30 | 0.5 | 0.6 | 0.22 |
| 6 | 1 | -1 | 1 | -1 | 50 | 0.5 | 0.6 | 0.22 |
| 7 | -1 | 1 | 1 | -1 | 30 | 0.7 | 0.6 | 0.22 |
| 8 | 1 | 1 | 1 | -1 | 50 | 0.7 | 0.6 | 0.22 |
| 9 | -1 | -1 | -1 | 1 | 30 | 0.5 | 0.4 | 0.28 |
| 10 | 1 | -1 | -1 | 1 | 50 | 0.5 | 0.4 | 0.28 |
| 11 | -1 | 1 | -1 | 1 | 30 | 0.7 | 0.4 | 0.28 |
| 12 | 1 | 1 | -1 | 1 | 50 | 0.7 | 0.4 | 0.28 |
| 13 | -1 | -1 | 1 | 1 | 30 | 0.5 | 0.6 | 0.28 |
| 14 | 1 | -1 | 1 | 1 | 50 | 0.5 | 0.6 | 0.28 |
| 15 | -1 | 1 | 1 | 1 | 30 | 0.7 | 0.6 | 0.28 |
| 16 | 1 | 1 | 1 | 1 | 50 | 0.7 | 0.6 | 0.28 |
| 17 | $-\alpha$ | 0 | 0 | 0 | 20 | 0.6 | 0.5 | 0.25 |
| 18 | $\alpha$ | 0 | 0 | 0 | 60 | 0.6 | 0.5 | 0.25 |
| 19 | 0 | $-\alpha$ | 0 | 0 | 40 | 0.4 | 0.5 | 0.25 |
| 20 | 0 | $\alpha$ | 0 | 0 | 40 | 0.8 | 0.5 | 0.25 |
| 21 | 0 | 0 | $-\alpha$ | 0 | 40 | 0.6 | 0.3 | 0.25 |
| 22 | 0 | 0 | $\alpha$ | 0 | 40 | 0.6 | 0.7 | 0.25 |
| 23 | 0 | 0 | 0 | $-\alpha$ | 40 | 0.6 | 0.5 | 0.19 |
| 24 | 0 | 0 | 0 | $\alpha$ | 40 | 0.6 | 0.5 | 0.31 |
| 25 - 30 | 0 | 0 | 0 | 0 | 40 | 0.6 | 0.5 | 0.25 |

advantages of the element is that any form of plate can be well managed with a simple mapping technique that can be defined as

$$x = \sum_{r=1}^{9} N_r x_r \quad \text{and} \quad y = \sum_{r=1}^{9} N_r y_r \tag{1}$$

where $(x, y)$ are the coordinates of any point within the element are, $(x_r, y_r)$ are the coordinates of $r^{\text{th}}$ nodal point and $N_r$ is the corresponding interpolation function of the element. In this element, Lagrangian interpolation function has been used for $N_r$.

The elegance of the formulation lies in the treatment of the inclusion of the shear deformation effect by taking the bending rotations as independent variables in the field, which are as follows

$$\begin{Bmatrix} \phi_x \\ \phi_y \end{Bmatrix} = \begin{Bmatrix} \theta_x - \dfrac{\partial w}{\partial x} \\ \theta_y - \dfrac{\partial w}{\partial y} \end{Bmatrix}$$

where $\phi_x$ and $\phi_y$ are the average shear rotation over the entire plate thickness and $\theta_x$ and $\theta_y$ are the total rotations

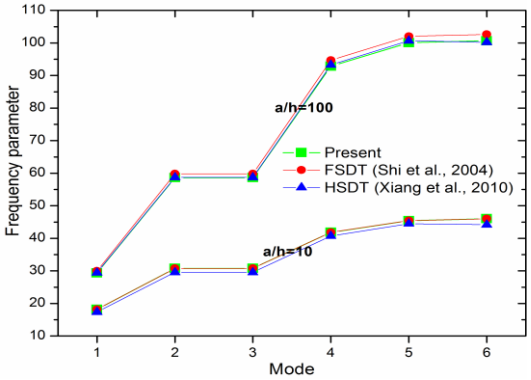


Fig. 2 Non-dimensional fundamental frequency $\lambda = \omega a^2/h\sqrt{\rho/E_2}$ of antisymmetric cross-ply $(0^o/90^o)_n$ square laminate

in bending.

Other independent field variables are $u$, $v$ and $w$, where $u$ and $v$ are the corresponding in-plane displacements, while $w$ is the transverse displacement.

The interpolation functions used for the representation of element geometry, Eq. (1), are used to express the displacement field at a point within the element in terms of nodal variables as

$$u = \sum_{r=1}^{9} N_r u_r\,; \qquad v = \sum_{r=1}^{9} N_r v_r\,; \qquad w = \sum_{r=1}^{9} N_r w_r\,; \tag{2}$$

$$\theta_x = \sum_{r=1}^{9} N_r \theta_{x_r}\,; \qquad \theta_y = \sum_{r=1}^{9} N_r \theta_{y_r}$$

For a laminate, the generalized stress-strain relationship with respect to its reference plane may be expressed as

$$\{\sigma\} = [D]\{\varepsilon\} \tag{3}$$

The generalized stress vector $\{\sigma\}$ in the above equation is

$$\{\sigma\}^T = \left[N_x\ N_y\ N_{xy}\ M_x\ M_y\ M_{xy}\ Q_x\ Q_y\right] \tag{4}$$

where, $N_x$, $N_y$, $N_{xy}$ are in-plane force resultants; $M_x$, $M_y$ are the bending moments in $x$ and $y$ directions; $M_{xy}$ is the twisting moment resultant; and $Q_x$, $Q_y$ are the transverse shear force resultants.

In the first-order shear deformation theory a shear correction factor $(k_c)$ is required to adjust the transverse shear stiffness for studying the static or dynamic problems of plates. The accuracy of solutions of the FSDT is strongly dependent on predicting better estimates for the shear correction factor. In this case, the shear correction factor is assumed to be 5/6.

The generalized strain in terms of displacement is written as,

$$\{\varepsilon\}^T = \left[\frac{\partial u}{\partial x}\ \ \frac{dv}{dy}\ \ \frac{\partial u}{\partial y}+\frac{\partial v}{\partial x}\ \ -\frac{\partial \theta_x}{\partial x}\ \ -\frac{\partial \theta_y}{\partial y}\ \ -\frac{\partial \theta_x}{\partial y}-\frac{\partial \theta_y}{\partial x}\ \ \frac{\partial w}{\partial x}-\theta_x\ \ \frac{\partial w}{\partial y}-\theta_y\right] \tag{5}$$

and

$$[D] = \begin{bmatrix} A_{11} & A_{12} & A_{16} & B_{11} & B_{12} & B_{16} & 0 & 0 \\ A_{12} & A_{22} & A_{26} & B_{12} & B_{22} & B_{26} & 0 & 0 \\ A_{16} & A_{26} & A_{66} & B_{16} & B_{26} & B_{66} & 0 & 0 \\ B_{11} & B_{12} & B_{16} & D_{11} & D_{12} & D_{16} & 0 & 0 \\ B_{12} & B_{22} & B_{26} & D_{12} & D_{22} & D_{26} & 0 & 0 \\ B_{16} & B_{26} & B_{66} & D_{16} & D_{26} & D_{66} & 0 & 0 \\ 0 & 0 & 0 & 0 & 0 & 0 & k_c.A_{55} & k_c.A_{54} \\ 0 & 0 & 0 & 0 & 0 & 0 & k_c.A_{45} & k_c.A_{44} \end{bmatrix} \quad (6)$$

where,

$A_{ij}$ , $B_{ij}$ , $D_{ij}$ are the extensional, extensional-bending and bending stiffness coefficients, which are defined in terms of the lamina stiffness coefficients (Kalita *et al*. 2018) genetically optimized skew laminates.

With the help of Eq. (2) and Eq. (5), the strain vector may be written as

$$\{\varepsilon\} = \sum_{r=1}^{9} \begin{bmatrix} \frac{\partial N_r}{\partial x} & 0 & 0 & 0 & 0 \\ 0 & \frac{\partial N_r}{\partial y} & 0 & 0 & 0 \\ \frac{\partial N_r}{\partial y} & \frac{\partial N_r}{\partial x} & 0 & 0 & 0 \\ 0 & 0 & 0 & -\frac{\partial N_r}{\partial x} & 0 \\ 0 & 0 & 0 & 0 & -\frac{\partial N_r}{\partial y} \\ 0 & 0 & 0 & -\frac{\partial N_r}{\partial y} & -\frac{\partial N_r}{\partial x} \\ 0 & 0 & \frac{\partial N_r}{\partial x} & -N_r & 0 \\ 0 & 0 & \frac{\partial N_r}{\partial y} & 0 & -N_r \end{bmatrix} \begin{Bmatrix} u_r \\ v_r \\ w_r \\ \theta_{x_r} \\ \theta_{y_r} \end{Bmatrix} \quad (7)$$

or, $\{\varepsilon\} = \sum_{r=1}^{9} [B]_r \{\delta_r\}_e$

or, $\{\varepsilon\} = [B]\{\delta\}$

Where $[B]$ is the strain matrix containing interpolation functions and their derivatives and $\{\delta\}$ is the nodal displacement vector having order $45 \times 1$

Once the matrices $[B]$ and $[D]$ are obtained, the stiffness matrix of the plate element $[K]$ can be easily derived by the virtual work method and it may be expressed as

$$[K]_e = \int_{-1}^{+1} \int_{-1}^{+1} [B]^T [D][B] \; |J| \; d\xi \, d\eta \quad (1)$$

In the above equation, the Jacobean $|J|$ is derived from Eq. (1) by taking the derivatives of the co-ordinates Eq. (7). The integration is carried out numerically following Gauss quadrature technique.

Similarly, the consistent mass matrix of an element can be derived and it may be expressed as

$$[M] = \rho h \int_{-1}^{+1} \int_{-1}^{+1} \left[ [N_u]^T [N_u] + [N_v]^T [N_v] + [N_w]^T [N_w] + \frac{h^2}{12} \left[N_{\theta_x}\right]^T \left[N_{\theta_x}\right] + \frac{h^2}{12} \left[N_{\theta_y}\right]^T \left[N_{\theta_y}\right] \right] |J| d\xi d\eta \quad (2)$$

where,

$$[N_u] = \left[[N_r][N_0][N_0][N_0][N_0]\right]$$
$$[N_v] = \left[[N_0][N_r][N_0][N_0][N_0]\right]$$
$$[N_w] = \left[[N_0][N_0][N_r][N_0][N_0]\right]$$
$$\left[N_{\theta_x}\right] = \left[[N_0][N_0][N_0][N_r][N_0]\right]$$
$$[N_{\theta_y}] = \left[[N_0][N_0][N_0][N_0][N_r]\right]$$

where, $[N_0]$ = null matrix of the order 1×9

In Eq. (9), the first two terms of the mass matrix are associated with in-plane movements of mass and the third term indicates transverse movement of mass (which is usually found to contribute the major inertia) whereas the last two terms are associated with rotary inertia and their contribution becomes significant only in a plate having higher thickness. In this formulation, the effect of rotary inertia as well as transverse and in-plane movements of mass are considered.

The element stiffness matrix and mass matrix having an order of forty-five are evaluated for all the elements and they are assembled together to form the overall stiffness matrix $[K_0]$ and mass matrix $[M_0]$. Once $[K_0]$ and $[M_0]$ are obtained the equations of motion of the plate may be expressed as

$$\{[K_0] - \omega^2 [M_0]\}\{\delta\} = 0 \quad (3)$$

After incorporating the boundary conditions in the above equation it is solved by the simultaneous iterative technique to get frequency $\omega$. Unless otherwise stated, all the frequency parameters are reported in this manuscript in non-dimensional form as,

$\lambda = \omega a^2 \sqrt{\rho h / D_0}$ , where, $D_0 = \frac{E_2 h^3}{12(1-\upsilon_{12}\upsilon_{21})}$

### *2.2 Response surface methodology*

Response surface methodology (RSM) generates an approximate equation relating the independent (input) parameters to the dependent (output) parameters. The inherent statistical and mathematical analysis fits an equation of the following form,

$$y = f(x_1, x_2, x_3, \ldots \ldots x_k) + \varepsilon \quad (4)$$

Here, $f$ denotes the approximate response surface and $\varepsilon$ is the normally distributed statistical error. $x's$ represents each independent parameter while $k$ is the maximum number of independent parameters. In general, a second-order models may be fitted as

$$y = \beta_0 + \sum_{i=1}^{k} \beta_i x_i + \sum_{i=1}^{k} \sum_{j>i}^{k} \beta_{ij} x_i x_j + \sum_{i=1}^{k} \beta_{ii} x_i^2 + \varepsilon \quad (5)$$

In this work, the central composite design (CCD) of RSM design is used. These designs consist of three distinct types of design points-two-level factorial design points, axial design points and center design points. The two-level factorial design points are coded as $\pm 1$; axial design points are coded as $\pm\alpha$ and center design points are coded as 0.

The full or partial two-level factorial design points forms the core while the axial design points lie outside the design space to offer rotatability to the design. This allows the response to predicted with equal variance irrespective of the direction from the centre of the design space. In general, the axial points, $|\alpha| > 1$. For a CCD design with full factorial core, the axial points can be calculated as (Rahman *et al*. 2017)

$$|\alpha| = \sqrt[4]{[2^k]} \tag{6}$$

Four parameters namely $\frac{E_1}{E_2}$, $\frac{G_{12}}{E_2}$ , $\frac{G_{23}}{E_2}$ and $\upsilon_{12}$ are studied to find their effect on fundamental frequency, $\lambda_1$ and frequency separation, $\lambda_{21}$. Table 1 shows design points in non-randomized standard sequence based on the CCD. However, while fitting the training data to second-order RSM model, the design points are randomized. Randomizing the 30 trials or design points (16 factorial terms, 8 axial terms and 6 replicates of center point) allows each trial to become an equal participant in the study. This contributes in distinguishing a 'true and rigorous experiment' from an observational study or a quasi-experiment (Shadish *et al*. 2008). The 16 factorial terms form the core of the CCD design, while the 8 axial terms ensure that even the extreme axial runs are within the area of operability. This is why in CCD design the area of interest must be within the area of operability. Traditionally the experiment corresponding to the center point is conducted multiple times to account for experimental error. However, in this article, since a FEA simulation is used there is no variation in experiment values for a particular point even when it is repeated multiple times. If the same set of inputs are provided for a FEA simulation, it would return the same output on repeated trials. Thus, in context of the present manuscript, trial number 25-30 represent the same input and output.

The CCD model is constructed from these 30 design points by using the multiple regression fitting scheme. The difference between the FE design points ($y_i$) and the CCD RSM model predicted points ($\hat{y}_i$) is called residual.

$$\varepsilon_i = y_i - \hat{y}_i \tag{7}$$

The $\beta_i$ estimates in Eq. (12) are selected such that the sum of squares of the residuals is minimized. The sum of squares of the residuals is also commonly called as the sum of squares of the errors($SSE$).

$$SSE = \sum_{i=1}^{n} {\varepsilon_i}^2 \tag{8}$$

The statistically non-significant terms are screened and removed from the RSM model. This is done by using an analysis of variance (ANOVA) test, where the effect of each independent variable on total model variance is quantitatively evaluated.

$$F_A = \frac{SS_{model}/_k}{SS_{residual}/_{(n-k-1)}} \tag{9}$$

$F_A$ is the F-test value of any independent variable, $SS_{model}$ and $SS_{residual}$ are the sum of squares due to model and residual respectively, $n$ is the number of sample points, $k$ is the number of independent variables. If $F_A$ exceeds the selected criterion value, the particular independent variable has a significant effect on the dependent variable. The non-significant terms are dropped from the model by backward, forward or stepwise elimination. This is done by calculating the *p-value* and the *prob.>F* value. *P-value* is the probability associated with the F-test value. It signifies the probability of getting the particular F-test value if the term did not have an effect on the response. Thus lower the *p-value*, more is the significance of the term. In general, a significant term should have p-*value* less than 0.05 (Keblouti *et al*. 2017).

Additional criteria like $R^2$, *adjusted* $R^2$ and *predicted* $R^2$ should also be considered for accepting or rejecting a model (Kalita *et al*. 2017). These can be calculated as,

$$R^2 = 1 - \frac{SS_{residual}}{SS_{residual} + SS_{model}} \tag{10}$$

$$adj.R^2 = 1 - \frac{SS_{residual}/_{(n-k-1)}}{(SS_{residual} + SS_{model})/_{(n-1)}} \tag{11}$$

$$pred.R^2 = 1 - \frac{PRESS}{SS_{residual} + SS_{model}} \tag{12}$$

$PRESS$ is the predicted residual sum of squares, which is a measure of how the model fits the samples in the design space. $R^2$ means how well the model is predicting a trend. 0% indicates that the model explains no variability of the response data and 100% means all variability around its mean is accounted for. However, $R^2$ can sometimes be misleading. This is why the performance of the model in terms of the adjusted $R^2$ and predicted $R^2$ should also be taken into account. Artificial inflation of $R^2$, occurs through the addition of terms to the model, regardless, of their statistical significance. However, if statistically insignificant terms are added both adj. $R^2$ and predicted $R^2$ would decrease. For an acceptable solution, both should be within 20% of each other.

### *2.3 Genetic algorithm*

Genetic Algorithm (GA) is good at taking huge search spaces and navigating them, looking for optimal combinations of parameters and predicting solutions. It works on Darwin's principle of natural selection (Goldberg 2006). GA is superior to most conventional search techniques in three major ways. It does not get trapped in local optima as it performs parallel search throughout the population of solutions. Secondly rather than optimizing the parameters itself, GA works on chromosomes which are an encrypted form of a potential solution, effectively bringing about a faster convergence. Thirdly the algorithm uses a fitness score based on the objective function to predict a feasible solution, which invites better performing solutions to influence successive searches. The user typically chooses

Table 2 Adequacy of the RSM models

| Metamodel | $R^2$ | Adj. $R^2$ | Pred. $R^2$ | Adequate Precision | p-value | Box-Cox transformation parameter (Λ) |
|---|---|---|---|---|---|---|
| Eq. (20) | 0.9998 | 0.9997 | 0.9991 | 364.09 | 4.79e-26 | No transformation |
| Eq. (21) | 0.9999 | 0.9997 | 0.9992 | 372.87 | 3.33e-26 | No transformation |
| Eq. (24) | 1.0 | 1.0 | 1.0 | 22290.47 | 8.50e-66 | 2 |
| Eq. (25) | 1.0 | 1.0 | 1.0 | 7341.93 | 1.23e-56 | 2 |

the best structure from the last generation as the optimal solution if the algorithm is set to terminate after a certain tolerance level is reached. However, running the algorithm for a predetermined number of times is more common among researchers. In this case, the algorithm terminates when the total predetermined number of iterations is reached, and it reports back the best solution encountered among all the generations (Kalita *et al.* 2018). Several research groups like Killickap and co-workers (Kilickap and Huseyinoglu 2010) (Kilickap *et al*. 2011) (Yardimeden *et al*. 2014); Jafarian and co-workers (Jafarian *et al*. 2013) (Jafarian *et al*. 2015) (Jafarian *et al*. 2014) (Jafarian *et al.* 2016) have regularly used genetic algorithms for a variety of optimization problems.

## 3. Results and discussion

### *3.1 Validation of FE results*

In this section, an example from literature is independently reproduced using the finite element formulation described in section 2.1. An all side clamped square angle-ply (45/-45/45/-45) composite plate with different side-to-thickness ratios (a/h= 10 and 100) is considered. The relative material properties of each layer are $E_1/E_2$ = 25, $G_{12}$ = $G_{13}$= 0.5$E_2$, $G_{23}$ = 0.2$E_2$, $\nu_{12}$= 0.25. The first six natural frequencies obtained by the present formulation are presented in Fig. 2 along with the published results of Shi *et al.* (2004) and Xiang *et al*. (2010). The present results are in more agreement with those of Shi *et al*. (2004) as compared to Xiang *et al*. (2010), who has used higher order deformation theory (HSDT). Shi *et al*. (2004) incorporated the transverse shear effects by considering first order shear deformation theory (FSDT) of Mindlin. Though FSDT is not as accurate as HSDT for very thick plates, it is simple to implement and gives much better results than the CPT and hence is reliable for thin and moderately thick plates. Further, the computational cost of using FSDT is cheaper than using HSDT. In past, the authors have shown the current finite element formulation to be able to produce highly accurate results (< 0.5%) for various structures (Kalita *et al*. 2016) (Kalita and Haldar 2017).

### *3.2 Building the RSM model*

An all edges simply supported square 8-layer angle ply $[45/-45/45/-45]_s$ composite laminate with thickness ratio h/a=0.01 is selected. Based on the central composite design reported in section 2.2, a training data set of 30 samples is selected. Multiple regression fitting scheme of the training

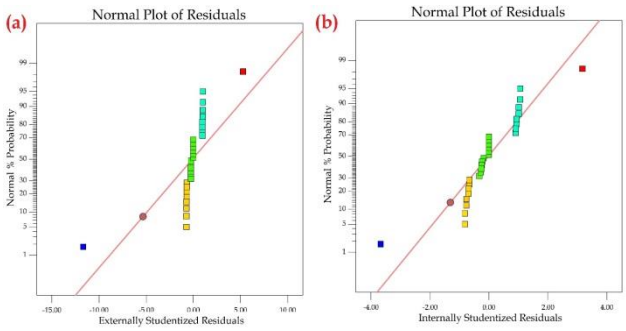


Fig. 3 Normal probability plot for metamodels built with untransformed data (a) fundamental frequency metamodel (b) frequency separation metamodel

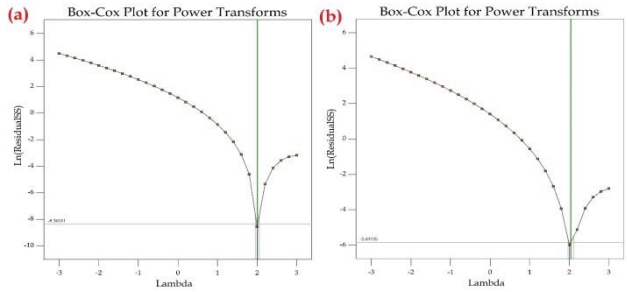


Fig. 4 Box-Cox plots for (a) fundamental frequency metamodel (b) frequency separation metamodel

dataset with respect to Eq. (12) leads to the development of non-linear second-order equations for fundamental frequency and frequency separation.

$$\begin{aligned}\lambda_1 = {} & 34.18650 + 1.63334\frac{E_1}{E_2} - 0.32732\frac{G_{12}}{E_2} - 0.25162\frac{G_{23}}{E_2} - 3.98572\,\upsilon_{12} \\ & + 0.01058\left(\frac{E_1}{E_2}\right)\left(\frac{G_{12}}{E_2}\right) + 0.01063\left(\frac{E_1}{E_2}\right)\left(\frac{G_{23}}{E_2}\right) + 0.00005\left(\frac{E_1}{E_2}\right)\upsilon_{12} \\ & - 0.54389\left(\frac{G_{12}}{E_2}\right)\left(\frac{G_{23}}{E_2}\right) - 0.00222\left(\frac{G_{12}}{E_2}\right)\upsilon_{12} + 0.00363\left(\frac{G_{23}}{E_2}\right)\upsilon_{12} \\ & - 0.00708\left(\frac{E_1}{E_2}\right)^2 + 0.43755\left(\frac{G_{12}}{E_2}\right)^2 + 0.45074\left(\frac{G_{23}}{E_2}\right)^2 + 7.96110\upsilon_{12}{}^2\end{aligned} \tag{13}$$

$$\begin{aligned}\lambda_{21} = {} & 42.93918 + 1.94325\frac{E_1}{E_2} + 4.26848\frac{G_{12}}{E_2} + 1.02359\frac{G_{23}}{E_2} - 2.85975\,\upsilon_{12} \\ & + 0.01412\left(\frac{E_1}{E_2}\right)\left(\frac{G_{12}}{E_2}\right) + 0.04045\left(\frac{E_1}{E_2}\right)\left(\frac{G_{23}}{E_2}\right) - 0.01212\left(\frac{E_1}{E_2}\right)\upsilon_{12} \\ & - 2.07287\left(\frac{G_{12}}{E_2}\right)\left(\frac{G_{23}}{E_2}\right) - 0.03778\left(\frac{G_{12}}{E_2}\right)\upsilon_{12} + 0.02352\left(\frac{G_{23}}{E_2}\right)\upsilon_{12} \\ & - 0.00853\left(\frac{E_1}{E_2}\right)^2 - 0.28821\left(\frac{G_{12}}{E_2}\right)^2 - 0.24067\left(\frac{G_{23}}{E_2}\right)^2 + 8.69585\upsilon_{12}{}^2\end{aligned} \tag{14}$$

The percentage residual (r) in the metamodels and the numerical finite element models is calculated as,

$$r\,\% = \frac{\lambda_{FEM} - \lambda_{RSM}}{\lambda_{FEM}} \times 100\% \tag{15}$$

The detailed statistics for checking the adequacy of the fitted RSM model with respect to $R^2$, adjusted $R^2$, predicted $R^2$, adequate precision and model *p-value* are reported in Table 2. Overall, the models appear to be excellent with high $R^2$, adjusted $R^2$, predicted $R^2$, adequate precision etc. However additional tests reveal that the model can be further improved. Many statistical tests and intervals are based on the assumption of normality. The assumption of normality often leads to tests that are simple, mathematically tractable, and powerful compared to tests

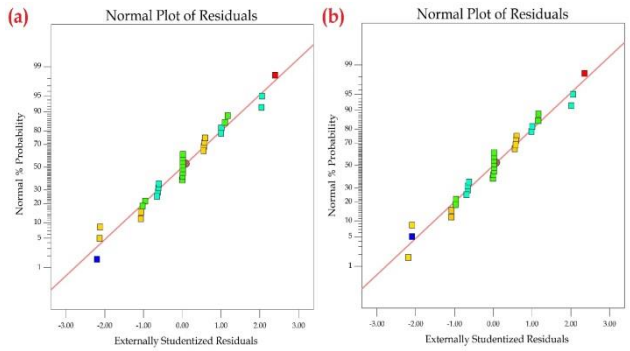


Fig. 5 Normal probability plot for metamodels built with Box-Cox transformed data (a) fundamental frequency metamodel (b) frequency separation metamodel

Table 3 ANOVA for metamodels built with Box-Cox transformed data

| Source | Fundamental Frequency | | | Frequency Separation | | |
|---|---|---|---|---|---|---|
| | Sum of Squares | F Value | p-value | Sum of Squares | F Value | p-value |
| Model | 83619120.77 | 27328299.82 | <0.0001 | 187083643.32 | 2967353.84 | <0.0001 |
| $\frac{E_1}{E_2}$ | 83616942.35 | 273275878.67 | <0.0001 | 186917172.18 | 29647134.25 | <0.0001 |
| $\frac{G_{12}}{E_2}$ | 937.50 | 3063.93 | <0.0001 | 137409.50 | 21794.67 | <0.0001 |
| $\frac{G_{23}}{E_2}$ | 695.75 | 2273.83 | <0.0001 | 16438.77 | 2607.37 | <0.0001 |
| $\upsilon_{12}$ | 0.01 | 0.02 | 0.8992 | 1002.94 | 159.08 | <0.0001 |
| $\frac{E_1}{E_2}\frac{G_{12}}{E_2}$ | 107.87 | 352.55 | <0.0001 | 2274.66 | 360.79 | <0.0001 |
| $\frac{E_1}{E_2}\frac{G_{23}}{E_2}$ | 99.99 | 326.79 | <0.0001 | 2237.62 | 354.91 | <0.0001 |
| $\frac{G_{12}}{E_2}\frac{G_{23}}{E_2}$ | 15.62 | 51.03 | <0.0001 | 343.43 | 54.47 | <0.0001 |
| $\left(\frac{E_1}{E_2}\right)^2$ | 321.49 | 1050.70 | <0.0001 | 6758.30 | 1071.94 | <0.0001 |
| $\left(\frac{G_{12}}{E_2}\right)^2$ | 6.87 | 22.45 | 0.0001 | 145.96 | 23.15 | 0.0001 |
| ${\upsilon_{12}}^2$ | 6.25 | 20.43 | 0.0002 | 145.63 | 23.10 | 0.0001 |
| Residual | 5.81 | | | 119.79 | | |
| Lack of Fit | 5.81 | | | 119.79 | | |

that do not make the normality assumption. Unfortunately, many real data sets are in fact not approximately normal. Normal probability plots of the externally studentized residuals for the fundamental frequency (Eq. (20)) and frequency separation (Eq. (21)) metamodels are shown in Fig. 3. Externally studentized residuals are the quotient resulting from the division of a residual by an estimate of its standard deviation. It is seen that the externally studentized residuals are not normally distributed and there are clusters of residuals at one place. This means the data may have ties, thus implying that the measuring resolution might not have been adequate. Box-Cox plots (Fig. 4) reveals that power transformations for the data may remove these inadequacies in the models. The minimum point of the curve generated by the natural log of the sum of squares of the residuals represents the appropriate transformation parameter. Thus, the training dataset is transformed using Box-Cox transformations calculated as,

$$y' = (y + C)^{\Lambda} \tag{16}$$

Where C is a constant and Λ is the power of

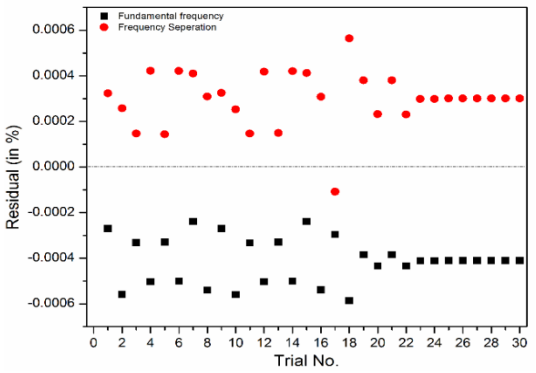


Fig. 6 Residuals for the training dataset for Box-Cox transformed data metamodels

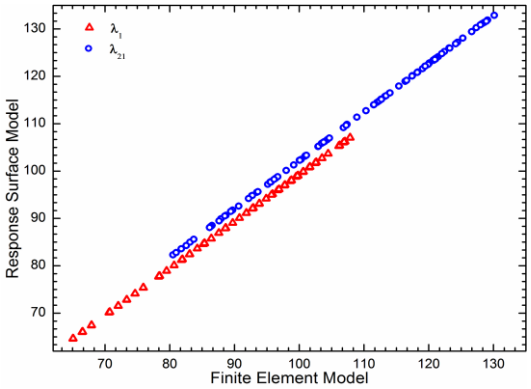


Fig. 7 Comparison of the original model and final metamodels

transformation. Again multiple regression fitting of the transformed training dataset with respect to Eq. (12) leads to the development of two new second-order equations for fundamental frequency and frequency separation. ANOVA is then performed on the metamodels to reduce them and remove the statistically insignificant terms. The final metamodels are reported in Eqs. (24) and (25) respectively. The detailed statistics like $R^2$, adjusted $R^2$ etc. are presented in Table 2, which shows considerable improvement over untransformed data models. The ANOVA results for metamodels stated as Eqs. (24) and (25) are reported in Table 3. Further Fig. 5 shows that a considerable improvements in normality of residuals is achieved by Box-Cox transformation.

$$\begin{aligned}{\lambda_1}^2 = {} & 202.58 + 186.56\frac{E_1}{E_2} + 67.47\frac{G_{12}}{E_2} + 60.37\frac{G_{23}}{E_2} - 0.48\,\upsilon_{12} + 2.60\left(\frac{E_1}{E_2}\right)\left(\frac{G_{12}}{E_2}\right) \\ & + 2.50\left(\frac{E_1}{E_2}\right)\left(\frac{G_{23}}{E_2}\right) - 98.79\left(\frac{G_{12}}{E_2}\right)\left(\frac{G_{23}}{E_2}\right) - 0.03\left(\frac{E_1}{E_2}\right)^2 - 49.53\left(\frac{G_{12}}{E_2}\right)^2 \\ & - 47.25\left(\frac{G_{23}}{E_2}\right)^2\end{aligned} \tag{17}$$

$$\begin{aligned}{\lambda_{21}}^2 = {} & 330.32 + 278.44\frac{E_1}{E_2} + 785.36\frac{G_{12}}{E_2} + 294.72\frac{G_{23}}{E_2} + 215.48\,\upsilon_{12} \\ & + 11.92\left(\frac{E_1}{E_2}\right)\left(\frac{G_{12}}{E_2}\right) + 11.83\left(\frac{E_1}{E_2}\right)\left(\frac{G_{23}}{E_2}\right) - 463.3\left(\frac{G_{12}}{E_2}\right)\left(\frac{G_{23}}{E_2}\right) \\ & - 0.16\left(\frac{E_1}{E_2}\right)^2 - 228.32\left(\frac{G_{12}}{E_2}\right)^2 - 228.06\left(\frac{G_{23}}{E_2}\right)^2\end{aligned} \tag{18}$$

Fig. 6 shows the percentage residual for the training dataset calculated using Eq. (22). It is seen that the metamodels have a prediction accuracy in the order of $10^{-4}$. The metamodels for fundamental frequency and frequency

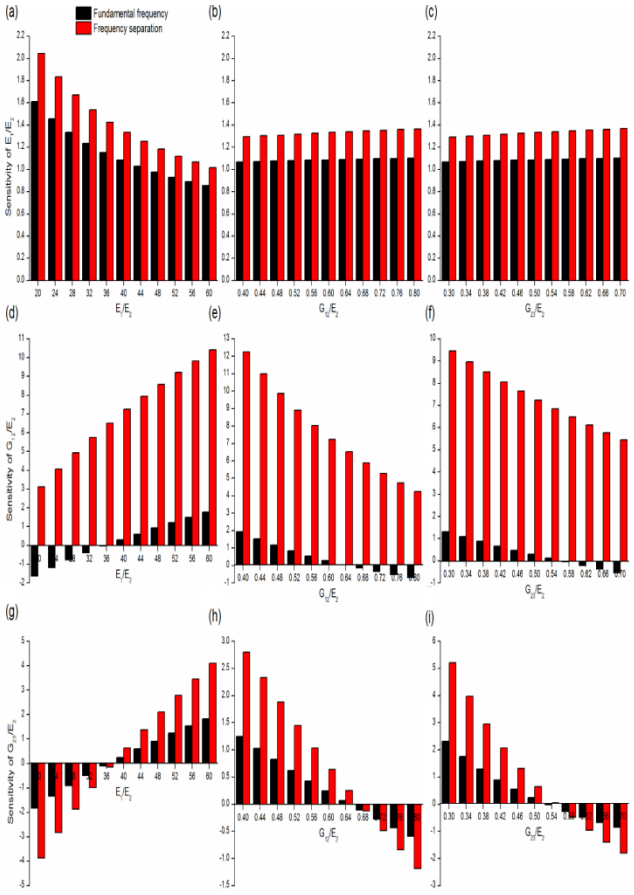


Fig. 8 Sensitivity of $\frac{E_1}{E_2}$, $\frac{G_{12}}{E_2}$, $\frac{G_{23}}{E_2}$ on fundamental frequency and frequency separation

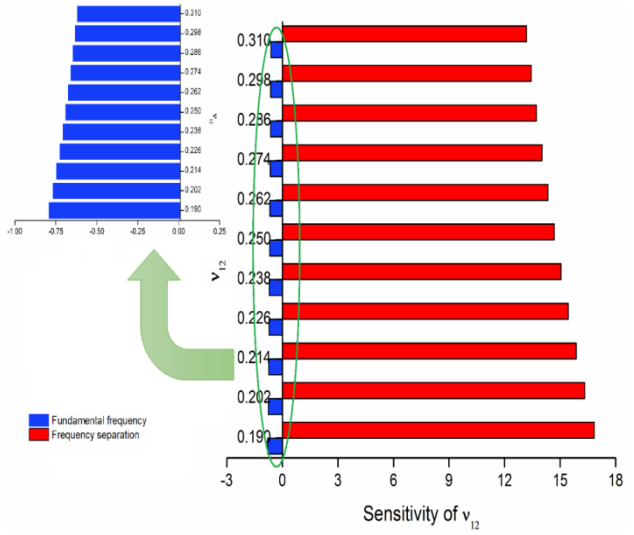


Fig. 9 Sensitivity of $\upsilon_{12}$ on fundamental frequency and frequency separation

separation are plotted against their respective finite element models in Fig. 7 for a randomly generated testing dataset of 100 sample points.

### *3.3 Sensitivity analysis*

Sensitivity analysis is a fundamental approach in determining which input responses have the most influence on the output variables. In this research, sensitivity analyses are performed by using a first-order derivate of the output response with respect to each independent variable. The individual sensitivity coefficients are then calculated by varying the independent variable in consideration within its selected range while keeping the other 3 independent variables at their respective mean levels.

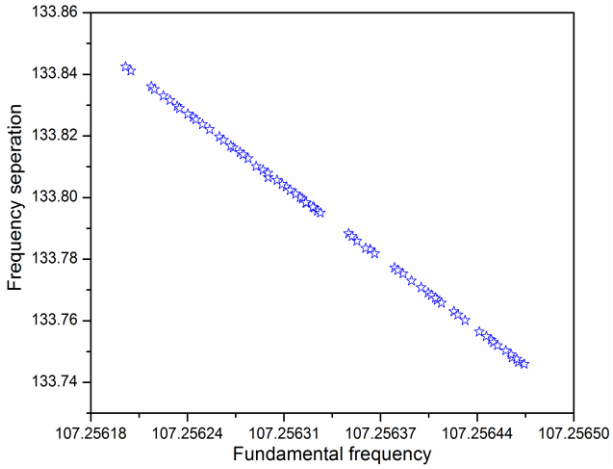


Fig. 10 Pareto front of the optimal solutions for maximized fundamental frequency and frequency separation

Fig. 8(a)-(c) illustrates the sensitivity of $\frac{E_1}{E_2}$ on $\lambda_1$ and $\lambda_{21}$ with variation in $\frac{E_1}{E_2}$, $\frac{G_{12}}{E_2}$ and $\frac{G_{23}}{E_2}$ respectively. Positive values of sensitivity means that $\lambda_1$ and $\lambda_{21}$ increases with corresponding increase in the value of the material property ratio whereas a negative value means that $\lambda_1$ and $\lambda_{21}$decreases with the corresponding decrease in material property ratio. In general, it is seen that $\lambda_1$ and $\lambda_{21}$ are very sensitive to $\frac{E_1}{E_2}$ and though positive, the sensitivity of $\frac{E_1}{E_2}$ with change in $\frac{G_{12}}{E_2}$ and $\frac{G_{23}}{E_2}$ is minimal. Fig. 8(d)-(f) illustrates the sensitivity of $\frac{G_{12}}{E_2}$ on $\lambda_1$ and $\lambda_{21}$ with variation in $\frac{E_1}{E_2}$, $\frac{G_{12}}{E_2}$ and $\frac{G_{23}}{E_2}$ respectively. Sensitivity of $\frac{G_{12}}{E_2}$ increases with corresponding increase in $\frac{E_1}{E_2}$ but decreases for increasing values of $\frac{G_{12}}{E_2}$ and $\frac{G_{23}}{E_2}$. Similarly in Fig. 8(g) sensitivity of $\frac{G_{23}}{E_2}$ increases with corresponding increase in $\frac{E_1}{E_2}$ but decreases for increasing values of $\frac{G_{12}}{E_2}$ and $\frac{G_{23}}{E_2}$ as seen in Fig. 8(h) and Fig. 8(i) respectively. As seen from Fig. 9, $\lambda_1$ and $\lambda_{21}$ are sensitive to changes in $\upsilon_{12}$ but there is no effect of variation of $\frac{E_1}{E_2}$, $\frac{G_{12}}{E_2}$ and $\frac{G_{23}}{E_2}$ on the sensitivity of $\upsilon_{12}$. Sensitivity of $\upsilon_{12}$ increases with the corresponding decrease in $\upsilon_{12}$. Overall, the sensitivity analysis plots reveal that $\lambda_{21}$ is more sensitive to any changes in material properties as compared to $\lambda_1$. $\frac{E_1}{E_2}$ is the most influential parameter whereas $\upsilon_{12}$ is least influential.

### *3.4 Optimization using GA*

The genetic algorithm solver '*gamultiobj*' provided in MATLAB Optimization Toolbox™ is used for solving this multi-objective optimization problem. The second-order non-linear equations developed using the RSM approach i.e., Eqs. (24) and (25) are used as the objective functions. An initial double vector type population of 100 individuals is selected. The creation function for the population is specified as 'feasible population'. This ensures that randomly created initial set of individuals satisfies the prescribed upper and lower bounds. A tournament section technique is then applied to randomly select the parents for the next generation. Tournament size is set at 2 i.e., two random individuals from generation 'n' are ranked against each other and the best amongst them in terms of scaled values from the fitness functions are selected as a parent for $(n+1)^{th}$ generation. Crossover fraction is set at 0.9 i.e. 90% of $(n+1)^{th}$ generation is produced by crossover and the remaining 10% is produced by mutation. A relatively low mutation prevents the loss of any key genetic material. Maximum generation limit and function tolerance are set at 200 and $10^{-6}$. It means that the genetic algorithm will terminate once 200 generations are reached or the weighted average change in the fitness function is less than $10^{-6}$. Optimal combinations predicted by the '*gamultiobj*' are reported in Fig. 10 in form of a Pareto front.

## 4. Conclusions

In this study, a multiobjective GA is used for designing composite plates for simultaneously maximized fundamental frequency and frequency separation between the first two natural modes. Instead of using a conventional variational method like Rayleigh-Ritz or finite element method for the numerical calculations, a novel metamodeling approach is used. The study successfully highlighted the potential of the proposed approach in a drastic reduction of computation cost at a very marginal loss of accuracy. Further, the effectiveness of Box-Cox transformation in augmenting the normality of a non-linear dataset is shown. An analysis of variance test is used for removing the insignificant terms from the metamodels, thereby making them more robust. Near-ideal values of descriptive parameters like $R^2$, adjusted $R^2$ and predicted $R^2$ depicted the excellent goodness of fit of a model. Sensitivity analysis of the metamodels revealed modulus ratio and Poisson's ratio to be the most and least influential parameters respectively. By carefully selecting the GA tuning parameters and incorporating the metamodels in it, a robust multiobjective optimization tool is developed to 'genetically engineer' the composite laminates for desired maximum frequency and frequency separation.

## References


Abu-Odeh, A.Y. and Jones, H.L. (1998), "Optimum design of composite plates using response surface method", *Compos. Struct.*, **43**(3), 233-242.

Boussaid, I., Lepagnot, J. and Siarry, P. (2013), "A survey on optimization metaheuristics", *Informat. Sci.*, **237**, 82-117.

Haykin, S.S. (2001), *Neural Networks: A Comprehensive Foundation*, Tsinghua University Press, China.

Heinonen, O. and Pajunen, S. (2011), "Optimal design of stiffened plate using metamodeling techniques", *J. Struct. Mech.*, **44**(3), 218-230.

Jafarian, F., Amirabadi, H. and Sadri, J. (2015), "Experimental measurement and optimization of tensile residual stress in turning process of Inconel718 superalloy", *Measure.*, **63**, 1-10.

Jafarian, F., Amirabadi, H., Sadri, J. and Banooie, H.R. (2014), "Simultaneous optimizing residual stress and surface roughness in turning of Inconel718 superalloy", *Mater. Manufact. Proc.*, **29**(3), 337-343.

Jafarian, F., Taghipour, M. and Amirabadi, H. (2013), "Application of artificial neural network and optimization algorithms for optimizing surface roughness, tool life and cutting forces in turning operation", *J. Mech. Sci. Technol.*, **27**(5), 1469-1477.

Jafarian, F., Umbrello, D., Golpayegani, S. and Darake, Z. (2016), "Experimental investigation to optimize tool life and surface roughness in Inconel718 machining", *Mater. Manufact. Proc.*, **31**(13), 1683-1691.

Ju, S., Shenoi, R.A., Jiang, D. and Sobey, A.J. (2013), "Multi-parameter optimization of lightweight composite triangular truss structure based on response surface methodology", *Compos. Struct.*, **97**, 107-116.

Kalita, K. and Haldar, S. (2017), "Eigenfrequencies of simply supported taper plates with cut-outs", *Struct. Eng. Mech.*, **63**(1), 103-113.

Kalita, K., Dey, P. and Haldar, S. (2018), "Robust genetically optimized skew laminates", *J. Mech. Eng. Sci.*

Kalita, K., Ramachandran, M., Raichurkar, P., Mokal, S.D. and Haldar, S. (2016), "Free vibration analysis of laminated composites by a nine node isoparametric plate bending element", *Adv. Compos. Lett.*, **25**(5), 108.

Kalita, K., Shivakoti, I. and Ghadai, R.K. (2017), "Optimizing process parameters for laser beam micro-marking using a genetic algorithm and particle swarm optimization", *Mater. Manufact. Proc.*, **32**(10), 1101-1108.

Keblouti, O., Boulanouar, L., Azizi, M.W. and Yallese, M.A. (2017), "Effects of coating material and cutting parameters on the surface roughness and cutting forces in dry turning of AISI 52100 steel", *Struct. Eng. Mech.*, **61**(4), 519-526.

Kilickap, E. and Huseyinoglu, M. (2010), "Selection of optimum drilling parameters on burr height using response surface methodology and genetic algorithm in drilling of AISI 304 stainless steel", *Mater. Manufact. Proc.*, **25**(10), 1068-1076.

Kilickap, E., Huseyinoglu, M. and Yardimeden, A. (2011), "Optimization of drilling parameters on surface roughness in drilling of AISI 1045 using response surface methodology and genetic algorithm", *Int. J. Adv. Manufact. Technol.*, **52**(1-4), 79-88.

Kim, D., Kim, D.H., Cui, J., Seo, H.Y. and Lee, Y.H. (2009), "Iterative neural network strategy for static model identification of an FRP deck", *Steel Compos. Struct.*, **9**(5), 445-455.

Mills, K.L., Filliben, J.J. and Haines, A.L. (2015), "Determining relative importance and effective settings for genetic algorithm control parameters", *Evolut. Comput.*, **23**(2), 309-342.

Mukhopadhyay, T., Dey, T.K., Chowdhury, R. and Chakrabarti, A. (2015), "Structural damage identification using response surface based multi-objective optimization: A comparative study", *Arab. J. Sci. Eng.*, **40**(4), 1027-1044.

Mukhopadhyay, T., Dey, T.K., Dey, S. and Chakrabarti, A. (2015), "Optimisation of fibre-reinforced polymer web core bridge deck. A hybrid approach", *Struct. Eng. Int.*, **25**(2), 173-183.

Pajunen, S. and Heinonen, O. (2014), "Automatic design of marine structures by using successive response surface

method", *Struct. Multidiscipl. Optim.*, **49**(5), 863-871.
Pan, S.S., Lei, S., Tan, Y.G. and Zhang, Z. (2011), "Reliability analysis for lateral stability of tongwamen bridge", *Steel Compos. Struct.*, **11**(5), 423-434.
Rahman, M.S., Islam, M.S., Do, J. and Kim, D. (2017), "Response surface methodology based multi-objective optimization of tuned mass damper for jacket supported offshore wind turbine", *Struct. Eng. Mech.*, **63**(3), 303-315.
Shadish, W.R., Clark, M.H. and Steiner, P.M. (2008), "Can nonrandomized experiments yield accurate answers? A randomized experiment comparing random and nonrandom assignments", *J. Am. Stat. Assoc.*, **103**(484), 1334-1344.
Shi, J.W., Nakatani, A. and Kitagawa, H. (2004), "Vibration analysis of fully clamped arbitrarily laminated plate", *Compos. Struct.*, **63**(1), 115-122.
Xiang, S., Shi, H., Wang, K.M., Ai, Y.T. and Sha, Y.D. (2010), "Thin plate spline radial basis functions for vibration analysis of clamped laminated composite plates", *Eur. J. Mech.-A/Sol.*, **29**(5), 844-850.
Yardimeden, A., Kilickap, E. and Celik, Y.H. (2014), "Effects of cutting parameters and point angle on thrust force and delamination in drilling of CFRP", *Mater. Test.*, **56**(11-12), 1042-1048.

*CC*